

UV circular polarisation in star formation regions: the origin of homochirality?

P.W.Lucas¹, J.H.Hough¹, Jeremy Bailey², Antonio Chrysostomou¹
T.M.Gledhill¹, Alan McCall¹

(1) Department of Physical Sciences, University of Hertfordshire, College Lane, Hatfield AL10 9AB, UK.
(2) Anglo-Australian Observatory, Post Office Box 296, Epping, New South Wales 121, Australia

Ultraviolet circularly polarised light has been suggested as the initial cause of the homochirality of organic molecules in terrestrial organisms, via enantiomeric selection of prebiotic molecules by asymmetric photolysis. We present a theoretical investigation of mechanisms by which ultraviolet circular polarisation may be produced in star formation regions. In the scenarios considered here, light scattering produces only a small percentage of net circular polarisation at any point in space, due to the forward throwing nature of the phase function in the ultraviolet. By contrast, dichroic extinction can produce a fairly high percentage of net circular polarisation ($\sim 10\%$) and may therefore play a key role in producing an enantiomeric excess.

1 Introduction

The homochirality of amino acids and sugars in terrestrial organisms is one of the more enduring mysteries concerning the origin of life. The sugars in DNA are exclusively D-sugars and structural proteins and enzymes contain only L-amino acids. Far from being a mere curiosity, homochirality appears to be a necessity for biochemical reactions to occur efficiently and may well be a prerequisite for life (Joyce et al. 1984). While some believe that homochirality may have arisen from an initially racemic mixture on the primordial Earth, the discovery of enantiomeric excesses of L-amino acids in the Murchison (Cronin & Pizzarello 1997; Engel & Macko 1997) and Murray (Pizzarello & Cronin 2000) meteorites argues for an extraterrestrial mechanism (see Bonner 1991). These excesses range from several per cent up to 15%. They are not now thought to have been produced directly by asymmetric photolysis (Pizzarello 2002, private comm.), since the circular dichroism of the amino acids is probably too small to produce such a large excess without dissociating $> 99\%$ of the molecules. Nevertheless it remains very possible that asymmetric photolysis introduces a smaller enantiomeric excess, which is then amplified by another physical or chemical mechanism.

In our view the most promising extraterrestrial mechanism is the asymmetric photolysis of prebiotic molecules by circularly polarised UV light in dusty nebulae around Young Stellar Objects (YSOs). This mechanism was suggested by Bailey et al.(1998) following the observation of nebulosity with 17% infrared circular polarisation (CP) in a dense cluster of YSOs in the well studied BN-KL region of the Orion Nebula BN-KL object and close to the highly obscured source IRc2. The crowded nature of the young star cluster in the vicinity of the circularly polarised nebulosity (designated BNKL SEBN) in Orion provides

a ready supply of young solar systems which could be undergoing asymmetric photolysis at the present time. Almost 20% CP has since been observed in another YSO, NGC6334V (Menard et al., 2000) but most other YSOs for which spatially resolved measurements exist exhibit somewhat lower CP ($\leq 5\%$). At present it appears that infrared CP ranges from 0% to about 20% in YSOs, though we caution that the observational database is still very small and the frequency of the higher value is unknown. We note that other possible sources of CP have been considered, eg. synchrotron or gyro-synchrotron radiation from a supernova remnant surrounding a pulsar (Rubenstein et al., 1983). However observed optical CP from the Crab Nebula is $< 1\%$, which is unsurprising given the difficulties of producing significant *net* CP in supernova remnants (Roberts 1984).

Unfortunately, the observations have to be made at infrared wavelengths because of the high extinction by the dusty medium in star formation regions. In this paper we calculate the net percentage of CP at ultraviolet wavelengths which can occur at points in the vicinity of YSOs and interstellar nebulae, considering a variety of scenarios.

The analysis of the Orion data by Bailey et al.(1998) and Chrysostomou et al.(2000) considered only light scattering as the mechanism to produce CP, focussing on the high CP which can be produced by scattering from aligned non-spherical dust grains. This was a natural assumption based on the observational data (see Section 4). However, CP can also be produced by dichroic extinction of linearly polarised light. This has been observed toward astrophysical nebulae (Martin et al., 1972) and stars (eg. Kemp & Wolstencroft 1972) and was attributed to dichroic extinction by a twisting magnetic field. CP attributed to this mechanism has also been observed towards YSOs, including the BN object in Orion. This source has CP of 1.6%, measured by Lonsdale et al.(1980) in a 10 arcsec beam. More recent spatially resolved observations (see Bailey et al., 1998; Chrysostomou et al., 2000) support this interpretation since the highly polarised nebulosity in the region is not close enough to the BN point source to contaminate the Lonsdale measurement with scattered light.

However, it remains unclear whether the CP in the nebulae is caused by dichroic scattering or by dichroic extinction of light which has been linearly polarised by scattering, a mechanism which can produce CP even if the magnetic field is uniform.

Dichroic extinction plays an important role in the calculations shown here, incorporating both multiple scattering and dichroic extinction. It has previously been modelled by Martin (1974) (not including scattered light) and at infrared wavelengths by Whitney & Wolff (2002) and Lucas (2003).

When the light from all parts of a system is summed, there can only be a net polarisation if there is some structural asymmetry. In many physical systems such asymmetries are small or average out over time. Brack (1998) noted that on Earth, net asymmetric photolysis and other electromagnetic interactions “probably cancel their effects on a time and space average.” It is therefore easy to produce models which lead to negligible net CP. In this paper we search for scenarios which can produce significant net CP, subject to the proviso that these appear to be realistic and consistent with the present knowledge of star formation regions.

2 Dichroic Scattering and Dichroic Extinction

In this work we consider two basic physical mechanisms which can generate a high degree of CP in star forming regions: scattering by aligned non-spherical grains (hereafter dichroic scattering) and dichroic extinction of linearly polarised light. Both mechanisms require the presence of non spherical grains which are at least partially aligned with respect to a common direction. The mechanism for initial alignment of the grains is a subject of debate (eg. Purcell 1979; Lazarian 1995, 2000; Roberge 1995) but it is generally accepted that non-spherical grains become aligned such that their axis of greatest rotational angular momentum precesses about the direction of the ambient magnetic field. There is abundant observational evidence for aligned grains in star forming regions, which produce linear polarisation through dichroic extinction or by emission at wavelengths from the ultraviolet through to the sub-millimeter (eg. Hough & Aitken 2003).

We note that scattering or absorption by optically active materials in the dust grains might also generate significant CP (if they are sufficiently abundant) but this is not considered here.

Before embarking on more complicated multiple scattering and extinction calculations (see Section 3) it is useful to provide an overview of CP production by individual spheroidal grains, which are the simplest non-spherical shape (see also Gledhill & McCall 2000). To calculate the (2×2 amplitude matrix, 4×4 Stokes matrix and 4×4 extinction matrix) the ampld.f and amplq.f codes of Mishchenko (see <http://www.giss.nasa.gov/~crmim>; Mishchenko, Hovenier & Travis 2000) were employed and to a lesser extent the codes of Barber & Hill (1990). Both works employ the T-matrix approach, expanding the electromagnetic wave as a series of spherical harmonics. Calculations were performed for grain axis ratios up to 3:1, considering a wide range of size parameters and arbitrary imaginary component of refractive index.

2.1 Dichroic Scattering

The polarisation state of the photon is described by the (I,Q,U,V) Stokes vector, defined relative to the scattering plane. It is modified by scattering as follows:

$$\begin{pmatrix} I \\ Q \\ U \\ V \end{pmatrix}_{scat} = \mathbf{Z} \begin{pmatrix} I \\ Q \\ U \\ V \end{pmatrix}_{inc}$$

where the Stokes matrix $\mathbf{Z} = \begin{pmatrix} Z_{11} & Z_{12} & Z_{13} & Z_{14} \\ Z_{21} & Z_{22} & Z_{23} & Z_{24} \\ Z_{31} & Z_{32} & Z_{33} & Z_{34} \\ Z_{41} & Z_{42} & Z_{43} & Z_{44} \end{pmatrix}$

The elements of \mathbf{Z} are all functions of the scattering angles and grain orientation angles. There are 3 independent angles for the oblate spheroids used in our calculation: photon polar deflection angle, D ; grain polar orientation, β ; and grain azimuthal orientation (α), which is defined relative to the azimuthal photon deflection angle. $\beta = 90^\circ$ presents the most elliptical cross section to the incident photon in the case of oblate spheroids, while $\beta = 0^\circ$ corresponds to a circular cross section. Full details of the definitions are given by Lucas (2003).

The ratio V/I gives the degree of circular polarisation, with positive V representing left-handed polarisation (LCP), and negative V representing right-handed polarisation (RCP), for a thumb pointing in the photon's direction of flight (i.e. along the Poynting vector).¹ Contributions to a Stokes vector from different sources of radiation are linearly additive, so equal quantities of LCP and RCP simply cancel out.

A photon which is scattered by a non-spherical dust grain can gain high CP (defined as $> 10\%$) owing to the phase difference between contributions to the electromagnetic field originating from different parts of the grain. By contrast, spherical grains can produce CP only from multiple scattering and even then usually at a low level (eg. Shafter & Jura 1980; Fischer, Henning & Yorke 1994; Lucas & Roche 1998). The degree of CP depends upon the direction of scattering and the orientation of the grain. In general, however, the greater the departure from spherical shape, the higher the CP (see Gledhill & McCall 2000). For simple grain shapes like spheroids and ellipsoids, small deflection angles always produce low CP, as well as low LP. The size parameter, x , is defined by $x = 2\pi a/\lambda$, where λ is the wavelength and a is the grain dimension (defined here as the radius of the equivalent surface area sphere).

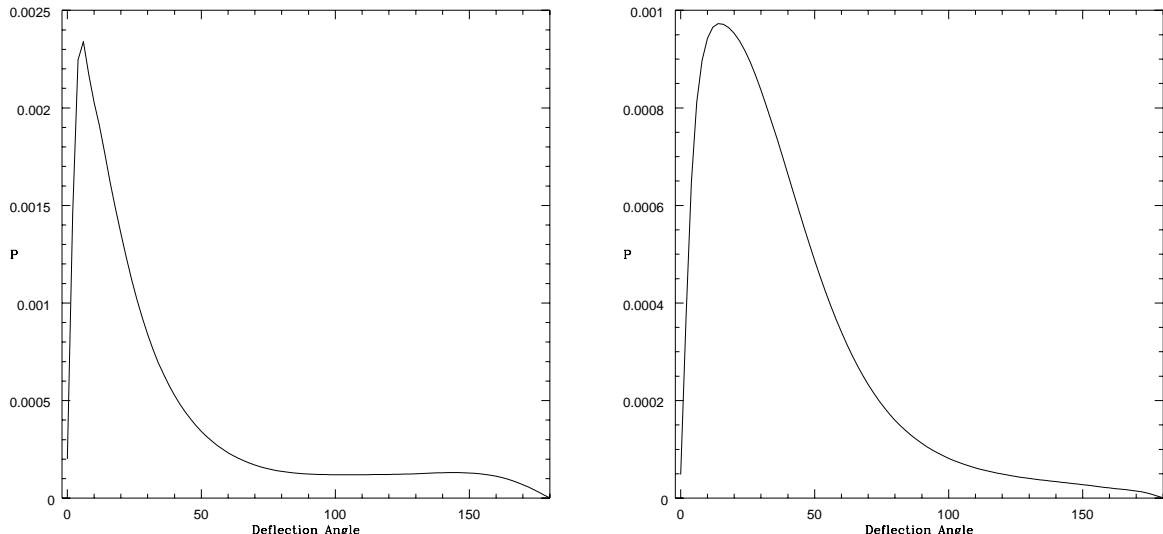


Figure 1. Phase function for dust in the envelope of a YSO, showing the relative probability of scattering through different deflection angles. The calculation uses the SACS2 mix (see section 3.1) and an unpolarised beam at $\lambda = 0.22 \mu\text{m}$ for oblate spheroids with a 3:1 axis ratio. The plotted functions are averaged over all azimuthal scattering angles and weighted by the available solid angle at each deflection angle, which is proportional to $\sin(D)$. (left) plot for face on orientation to the incident ray ($\beta = 0^\circ$), illustrating the highly forward throwing phase function. (right) edge on orientation ($\beta = 90^\circ$), showing slightly weaker forward scattering due to the smaller cross section.

Dust grains which are significantly larger than the photon wavelength ($x > 1$) have a high probability of causing small angle deflection, producing low CP (see Figure 1). For scattering at the typical wavelengths of chiral bands in prebiotic molecules (150 to 220 nm) this is likely to be the situation for dust grains in star formation regions, where

¹The sense of positive V was erroneously stated as right-handed in Lucas (2003), but plots of positive and negative V in that work remain correct.

the maximum grain size is larger than in the diffuse interstellar medium, perhaps reaching $0.8 \mu\text{m}$ in equivalent radius in the circumstellar envelopes of YSOs (Minchin et al., 1991a; 1991b). We note that if a photon is deflected through a large angle, CP close to 100% can in principle be produced by large grains ($x \geq 1.5$ and axis ratio 2:1, see Gledhill & McCall 2000). However, this is unlikely to occur in astrophysical media where there is usually a range of grain sizes. The reason is that grains of different size produce maximum CP at different grain orientations and scattering angles, so that the CP at any particular scattering angle is usually well below 50% (see section 3.1).

At very small size parameters ($x \ll 1$), appropriate to very small dust grains, the distribution of scattered light (phase function) is more isotropic but the CP is low ($< 10\%$) for all scattering angles (see Figure 8 of Gledhill & McCall 2000) unless the grains are very absorptive. For small and highly absorptive grains there is little scattered light due to the very low albedo. If dichroic scattering is to produce efficient asymmetric photolysis in a star forming region both high CP and a non-negligible albedo are desirable, so that the scattered light dominates the radiation field. This is most likely to occur if the optically dominant grain size is comparable to or slightly smaller than the wavelength, i.e. $x \sim 1$.

2.2 Dichroic Extinction

The polarisation state of a photon (this time defined in the reference frame of the grains, with positive Stokes Q parallel to the axis of grain alignment) is modified by dichroic extinction when travelling a distance s through a uniform cloud with grain number density n as follows (see Whitney & Wolff 2002; Martin 1974):

$$(2) \quad I_{ext} = 0.5\{(I_{inc} + Q_{inc})\exp[-n(K_{11} + K_{12})s] + (I_{inc} - Q_{inc})\exp[-n(K_{11} - K_{12})s]\}$$

$$(3) \quad Q_{ext} = 0.5\{(I_{inc} + Q_{inc})\exp[-n(K_{11} + K_{12})s] - (I_{inc} - Q_{inc})\exp[-n(K_{11} - K_{12})s]\}$$

$$(4) \quad U_{ext} = \exp[-nK_{11}s].\{U_{inc}\cos(nK_{34}s) - V_{inc}\sin(nK_{34}s)\}$$

$$(5) \quad V_{ext} = \exp[-nK_{11}s].\{V_{inc}\cos(nK_{34}s) + U_{inc}\sin(nK_{34}s)\}$$

where K_{11} , K_{12} and K_{34} are the 3 independent elements of the 4×4 extinction matrix which acts on the Stokes vector. For spheroids the K_{ij} elements are function of the grain azimuthal and polar orientation angles (α and β respectively, see Mishchenko et al., 2000.)

For unpolarised light eqs.(2-5) merely lead to light which is linearly polarised in Stokes Q , parallel to the axis of grain alignment. Equs. (4-5) show that CP is produced only by conversion of Stokes U to Stokes V due to the birefringence term K_{34} . This term acts by introducing a phase difference between the components of the electromagnetic wave oscillating parallel to and perpendicular to the axis of grain alignment. Hence, dichroic extinction only leads to CP if there is prior linear polarisation in Stokes U . Two obvious ways of producing this are by scattering or by prior dichroic extinction with a different grain alignment axis. The latter case would occur if light is passed through a nebula with a twisting magnetic field (Martin 1974) or by passing light through two spatially separated nebulae with different magnetic field directions.

CP production by dichroic extinction is most efficient at wavelengths significantly larger than the grain size ($x < 1$), where the ratio K_{34}/K_{11} is high (see Figure 2). This initially appeared discouraging for the production of high CP at $\lambda \leq 0.22 \mu\text{m}$ in star

formation regions. We note, however, that high CP can be produced even at UV wavelengths where K_{34}/K_{11} is low, provided that the ratio of birefringence to linear dichroism (K_{34}/K_{12} terms) is not far below unity and the optical depth of the medium is greater than unity.

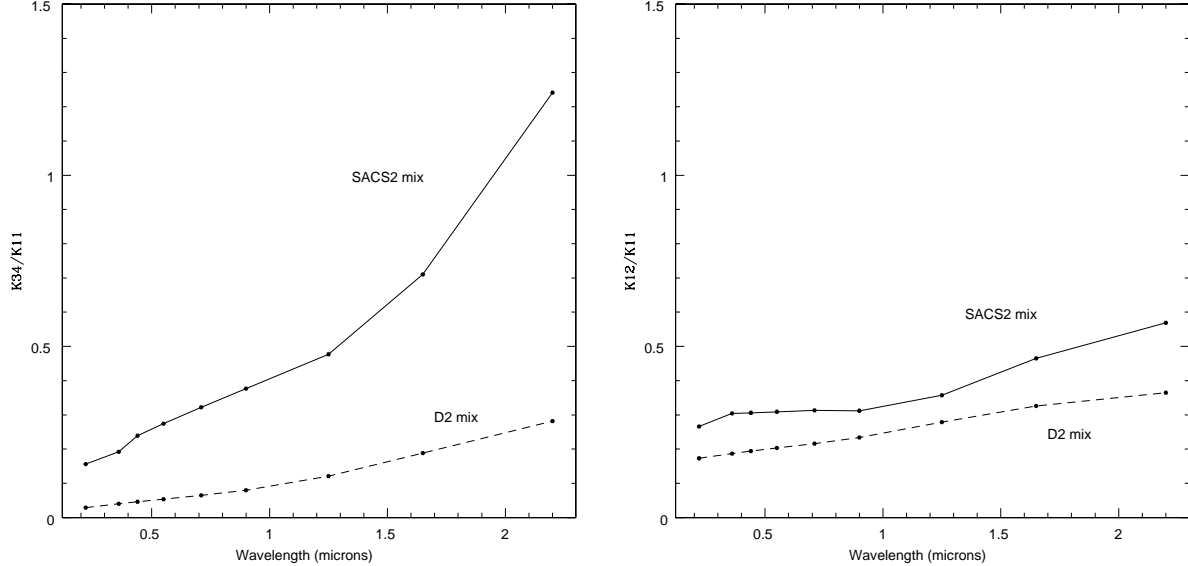


Figure 2. (left) Plot of K_{34}/K_{11} (birefringence/neutral extinction) as a function of wavelength. The calculations are for the larger grain mixtures found in the circumstellar envelopes of YSOs (see section 3.1 for definitions of grain mixtures), for oblate spheroids with a 3:1 axis ratio. Birefringence is weak in the ultraviolet. However, it is stronger for the 'shiny' SACS2 mix than the 'dirty' D2 mix. (right) Plot of K_{12}/K_{11} (dichroic extinction/neutral extinction). Both K_{34}/K_{11} , K_{12}/K_{11} are calculated in the reference frame defined by the grain alignment (see text).

This point is illustrated in Figure 3 for a 220 nm light ray which is initially 100% linearly polarised in Stokes U. It shows the change in the Stokes vector as it passes deep into an optically thick cloud of oblate spheroid grains with axis ratio 3:1, which are perfectly aligned with the Stokes Q direction and oriented edge on to the incident photon. The chosen grain mixture is composed of silicate and small amorphous carbon grains (the SACS1 mix, see Section 3) whose size distribution is plausible for the interstellar environment of star forming dark clouds. For this mix $K_{34}/K_{11} = 0.181$, while $K_{12}/K_{11} = 0.294$ (evaluated at $\alpha = 0^\circ$, $\beta = 90^\circ$).

As optical depth, τ , increases from zero, the K_{34} term gradually converts Stokes U to Stokes V, while the K_{12} term converts U to Q at a similar rate. Since K_{12}/K_{11} is small, a high CP can be generated at $1 < \tau < 7$, for it is not until $\tau > 7$ that essentially all the polarisation is forced into the Stokes Q plane, where oscillating electric waves suffer least extinction. In this example a CP of 37.5% occurs at $\tau = 3$, at which point 5% of the original flux remains in the beam. For grain mixtures with very low absorptivity and similar size distribution the maximum CP approaches 50%. However, this calculation, which is similar to those of Martin (1974), does not include the diluting effect of scattered light (see Section 3.3).

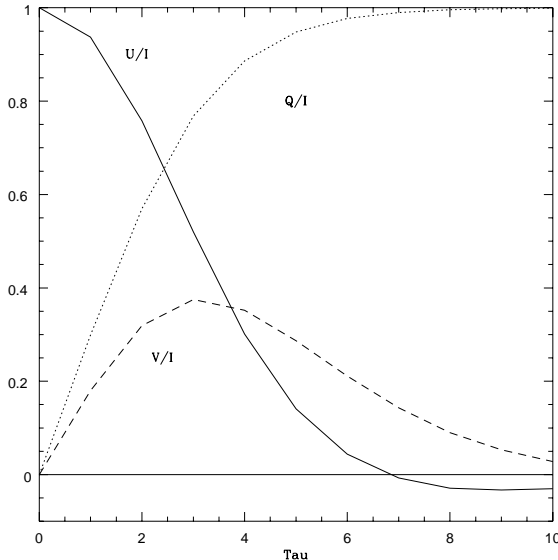


Figure 3. Circular Polarisation from Dichroic Extinction. The example calculation is at $0.22\ \mu\text{m}$, showing the effect of small, shiny grains (SACS1 mix) as a function of optical depth on a ray which is initially 100% linearly polarised (see text). The incident ray is polarised in the U plane and the grains are aligned with the Q plane. (solid curve) Stokes U/I ; (dotted curve) Q/I ; (dashed curve) V/I .

3 Monte Carlo modelling

We employ the Monte Carlo method to simulate multiple scattering and extinction in YSOs and in interstellar nebulae. The 2-D scattering code used here for axisymmetric nebulae is described in Lucas (2003). Efficient 3-D models for less symmetric nebulae have been implemented for YSO modelling using forced scattering (Wood & Reynolds 1999; Lucas et al., 2003) but here we treat asymmetric nebulae in a very simple way, which is described later. In summary, the code randomly generates millions of photons at the stellar surface (assuming uniform surface brightness) and each follows a random path through the nebula, perhaps scattering several times before it escapes the system or is absorbed. At present the code handles only perfectly aligned oblate spheroids. Perfectly aligned oblate spheroids appear to yield the highest degrees of CP (Gledhill & McCall 2000; Whitney & Wolff 2002), since the shape presented to the wavefront does not change with rotation. Rotation (in the case of prolate spheroids) and precession both change the shape presented to the wavefront, leading to a reduction in the CP produced after averaging over a full period.

Arbitrary magnetic field structures can be included, these being specified algebraically. The **Z** and **K** matrix elements and the amplitude matrix elements needed in the phase function are stored as large look up tables, sampling all the relevant angles every 2° . This interval is the maximum for simulations in the ultraviolet, where the phase function is strongly peaked in the forward scattering direction (see Figure 1).

The millions of photons output from the system are used to construct polarimetric images of the nebula as seen in the far field, for comparison with telescopic observation from Earth. We also calculate the net CP received at points close to the nebula in the near field, summing the contributions to the radiation field of LCP and RCP that are incident from all directions. Note that we have not extended the calculations to wavelengths

shorter than $0.22 \mu\text{m}$ (appropriate for the longer wavelength chiral bands) because: (a) computation for the shorter wavelength chiral bands near $0.15 \mu\text{m}$ is very demanding in several respects and; (b) the luminous flux from all but very hot stars declines steeply at shorter wavelengths (see Bailey et al., 1998).

3.1 Dust Mixtures

The size, shape and composition of dust in star formation regions is not known with precision and may well vary in different environments. In this section we define four dust grain mixtures which span most of the plausible range of size and of absorptivity that could be encountered. The two smaller mixtures are better suited to production of CP by dichroic extinction than their larger counterparts. The two larger grain mixtures have a size distribution specifically designed to maximise CP production by dichroic scattering.

There is a large literature on the subject which assists in constructing plausible dust models. Pollack (1994) gives a cogent analysis of the possible grain compositions in cold molecular clouds and grain sizes have been analysed by Kim, Martin & Hendry (1994), among others. The size distribution in the diffuse interstellar medium appears to be well modelled grains with sizes $0.005 < a < 0.25 \mu\text{m}$ and a power law index $k=3.5$ in that range, so that $n(a) \propto a^{-k}$ (Mathis, Rumpl & Nordsieck 1977). Interstellar grains in dark clouds are known to be slightly larger than in the diffuse interstellar medium (eg. Whittet 1992): the ratio of total to selective extinction at visible wavelengths (R_V) rises from 3.1 in the diffuse medium to between 4 and 5.5 in different dark clouds; also the degree of LP due to extinction, described by the Serkowski law, peaks at a slightly longer wavelength in dark clouds. However, Cardelli, Clayton & Mathis (1989) showed that the wavelength dependence of *infrared* extinction in dark clouds is similar to that of the diffuse medium, strongly implying that there are few grains with $a > 1 \mu\text{m}$. For interstellar dust in dark clouds we adopt the following basic size distribution: $0.005 < a < 0.3 \mu\text{m}$, retaining the $k=3.5$ power law index of Mathis, Rumpl & Nordsieck. An axis ratio of 3:1 is adopted for these oblate spheroids (see below).

We define two different mixtures of these relatively small grains for use in the medium of dark clouds.

- the D1 mix: a highly absorptive mixture of unspecified composition with refractive index $n=1.5-0.2i$.
- the SACS1 mix: a more reflective mixture consisting mostly of 'astronomical silicate' with $0.005 < a < 0.3 \mu\text{m}$ (refractive index at each wavelength from Draine 1985) and an additional component of small amorphous carbon grains (refractive indices from Preibisch et al., 1993), only in the size range $0.005 < a < 0.03 \mu\text{m}$. This grain composition is not intended to be realistic but merely representative of mixtures with relatively low absorption. The small carbon grains (whose size is limited by hydrogenation and chemical sputtering in dense clouds, see Sorrell (1990)) have very little influence on the polarisation of scattered light, since they are almost purely absorbing. They serve to reduce the albedo of the silicate mixture to 0.61 at $\lambda = 0.22 \mu\text{m}$, where it would otherwise exceed 0.9 for a mixture consisting only of reflective substances such as silicates or water ice.

In the denser environment of the circumstellar envelopes of YSOs, the grains may well be larger than in the dark cloud medium. The parameter space of size, axis ratio, composition, deflection angle and grain orientation was explored with ampltf.f code to find grain mixtures which were capable of reproducing the high CP observed by Bailey et al. (1998)

and Menard et al.(2000) at $2.2 \mu\text{m}$ via single dichroic scattering, while also producing the observed high LP ($> 60\%$ at $3 \mu\text{m}$) (Minchin et al., 1991a) and a non-negligible albedo ($\gtrsim 0.2$) at $2.2 \mu\text{m}$. It was found that for power law index $k=3.5$, the grain axis ratio must approach 3:1 and the grain size must extend up to $0.75 \mu\text{m}$ to produce CP of 17% or more over at least a modest range of grain orientations and scattering angles. This upper size limit is in close agreement with the value of $0.8 \mu\text{m}$ independently suggested by Minchin et al.(1991b) by analysing the linear polarisation in the BN-KL region of Orion. Including even larger grains reduces the CP produced by the mixture, since in such grains the phase difference between the parallel and perpendicular components of the scattered radiation field exceeds 180° , causing a CP reversal. The 3:1 axis ratio is larger than is usually assumed in astrophysical nebulae, but this may be part of the reason for the very high observed CP. Alternatively, the axis ratio may be smaller than 3:1 if dichroic extinction rather than dichroic scattering is responsible for the observed CP (see Section 4). However, the aim of this paper is to test the physical feasibility of producing high UV CP rather than to calculate the typical values of CP in the radiation field of dark clouds. A large axis ratio aids the production of high CP by both mechanisms. Chrysostomou et al.(2000) found that for perfectly aligned grains a 2:1 axis ratio was sufficient to produce the *average* value of CP ($\sim 10\%$) in the BNKL-SEBN nebula in Orion, which we confirm (and up to 17% if the combination of grain orientation and scattering angle is precisely optimal). A preliminary calculation by Bailey et al.(1998) showed that in the case of extremely absorptive grains ($n=1.5-0.4i$) an axis ratio of 2:1 would be also sufficient to reproduce the observed 17% CP over a wide range of grain orientations and scattering angles. However, our calculated albedo for that grain mixture is only 0.02 at $2.2 \mu\text{m}$, which is inconsistent with the brightness of the observed nebula.

We define two different mixtures of these relatively large grains for use in the envelopes of YSOs.

- the D2 mix: $0.005 < a < 0.75 \mu\text{m}$, $k=3.5$, $n=1.5-0.2i$.
- the SACS2 mix: identical to the SACS1 mix except that the silicate component has a size distribution $0.005 < a < 0.75 \mu\text{m}$. This mix has an albedo of 0.60 at $0.22 \mu\text{m}$.

For completeness we note that different values of k do not appear to increase CP.

3.2 Scenario 1 - a single high mass YSO

The first scenario that we model is the case of a single intermediate to high mass YSO, in order to examine the CP produced in the external radiation field, which would be experienced by a passing low mass YSO. High mass stars are not thought to be suitable sites for life (stellar lifetimes ≤ 100 Myr are too short for terrestrial style evolution and have comparable duration to the likely period of intense asteroid bombardment) but they dominate the UV radiation field in star formation regions (see Bailey et al., 1998). This is demonstrated by the observation of photoevaporating 'proplyd' envelopes around low mass stars, with cometary tails pointing away from the massive O-type stars at the centre of the Trapezium cluster (eg. O'Dell & Wen 1994). In the case of the BN-KL region there are dozens of low mass stars within a small fraction of a parsec which could be undergoing asymmetric photolysis if the radiation field has significant net CP.

The main features of a YSO are illustrated in Figure 4: Embedded YSOs with ages of order 10^5 yr consist of a central protostar surrounded by a relatively thin accretion disk of gas and dust a few hundred AU in extent, which is itself surrounded on scales of up

to several thousand AU by a large envelope which is slowly gravitating toward the disk and is optically thick even at near infrared wavelengths. The central protostar contains at least 90% of the mass of the system (Andre & Montmerle 1994) and the accretion disk has a central hole about the star extending out to several stellar radii in which the dust has sublimated (Hamann & Persson 1992; Hillenbrand et al., 1992), with the consequence that only a small fraction of the flux from the star is intercepted by the disk. The envelope contains a bipolar cavity centred on the star, which is cleared by the stellar wind and allows light from the star to escape the system along angles close to the rotation axis of the system with little or no extinction by dust. Hence the intensity and polarisation state of light escaping the system is a strong function of polar angle. Note that the embedded phase is much briefer in the most luminous YSOs, for which the above description may not apply.

A passing YSO which is directly illuminated by the central star along a line close to the rotation axis will receive a large unpolarised UV flux, which will efficiently destroy prebiotic molecules and leave no enantiomeric excess. However, a YSO passing close to the equatorial plane receives a much lower flux which is both linearly and circularly polarised.

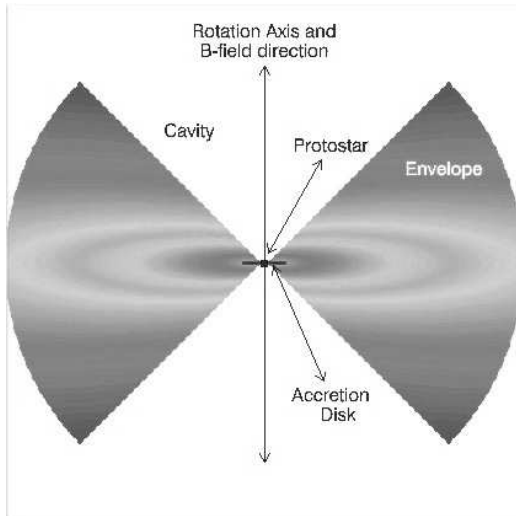


Figure 4: Schematic diagram of a Young Stellar Object. In this example the magnetic field is axial and parallel to the rotation axis of the system. The density of the envelope declines monotonically with distance from the protostar and distance from the disk plane. The density spans several orders of magnitude, as indicated by the wrapped greyscale shading. The cavity is taken to be evacuated.

3.2.1 Axial Field

The results of a simulation at $\lambda = 0.22 \mu\text{m}$ with the SACS2 mix are illustrated in Figure 5(a-f), for the case of an axial magnetic field. A B-field which is axial on scales of thousands of AU is the expected result because the gravitational collapse of molecular cloud cores with even quite low levels of ionisation goes preferentially along the field lines. An axial field has previously been observed on scales of thousands of AU (eg. Tamura, Hough & Hayashi 1995) but the observational database suggests that on smaller scales the field may be axial in some YSOs and toroidal in others (Wright 1994; Smith et al., 2000).

In this example the cavity is conical and has an opening angle of 45° to the vertical. The accretion disk is a flared structure in vertical hydrostatic equilibrium (see Shakura & Sunyaev 1973) with radius 400 AU, and density given by:

$$(6) \rho_{\text{disk}} = \begin{cases} \rho_0 (R/R_*)^{-15/8} \exp[-0.5(z/h)^2]; & 400 \text{ AU} > r > 20 R_* \\ = 0; & r < 20 R_* \\ = 0; & r > 400 \text{ AU} \end{cases}$$

where $R = \sqrt{r^2 + z^2}$ (cylindrical polar coordinates defined by the disk plane), R_* is the stellar radius, set at 2 solar radii (or ~ 0.01 AU), and h is the disk scale height, given by:

$$(7) h = h_0 (R/R_*)^{9/8}; h_0 = R_*/75$$

The size of the inner hole is taken from results in Chiang et al., 2001). Eqs.(6-7) describes the disk in all YSO simulations in this paper. In fact it has little influence on the output. The structural features which do affect model outputs most are the surrounding envelope, the system inclination and the evacuated cavity.

In this example the envelope density is given by:

$$(8) \rho_{\text{env}} = \begin{cases} C/R^{1.5} [1/((|z|/R)^v + 0.05)]; & 50 < r < 5000 \text{ AU} \\ = 0; & r < 50 \text{ AU} \end{cases}$$

C is a free parameter governing the optical depth from the star to the edge of the system, on lines of sight which do not intersect the accretion disk. In the results shown in Figure 5, C is set to a value which leads to optical depth $\tau_{60^\circ} = 3.4$, defined at inclination $i = 60^\circ$. v is a parameter describing the vertical gradient of the envelope, and was set to 2.0 in the results shown here, so that the envelope is a flattened structure as shown in Figure 4. Eq.(8) is a simple, empirically derived formalism, adopted following the discovery that the $R^{-1.5}$ power law seems to extend throughout the envelope in at least some YSOs (Lucas & Roche 1998).

The top panels of Figure 5 show the total flux from the system as seen in the far field, at inclination angles $i = 90^\circ$ and 72.5° . At 90° (viewing in the equatorial plane) the system appears as a bipolar nebula, with the central star entirely obscured. At $i = 72.5^\circ$ ($\cos(i) = 0.3$) the star is still obscured but the image is dominated by light scattered through small angles in the inner parts of the envelope. The middle panels of Figure 5 show the CP produced by scattering alone, and the lower panels show the CP after including the effect of dichroic extinction. The left-middle panel shows a quadrupolar symmetry: the sign of CP alternates between adjacent quadrants of the image. This has been observed in several YSO nebulae (eg. Chrysostomou et al., 1997) and is simply due to alternations in the sign of the Stokes U component (part of which is converted to Stokes V) as perceived in the scattering plane. The bottom panels show that dichroic extinction significantly modifies the CP, even reversing the sense of it in places where the optical depth is high (close to the equatorial plane).

High CP occurs in parts of the images at both $i = 90^\circ$ and 72.5° but not in the regions where the image is brightest. In this example a conical cavity with an opening angle of 45° was used, in order to ensure adequate illumination of the regions at fairly low latitude

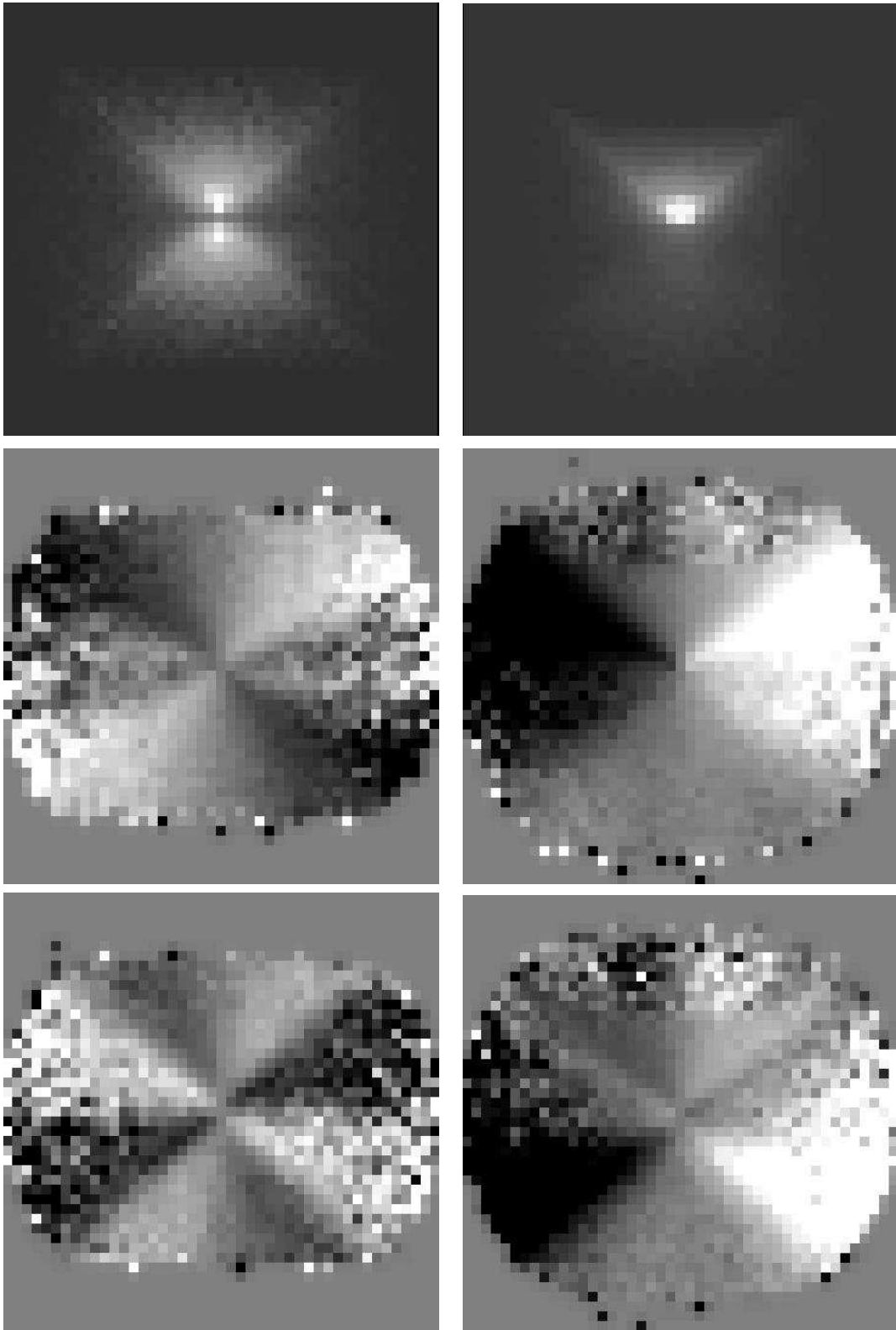


Figure 5. Simulation of a YSO with an axial magnetic field as viewed in the far field. ($\lambda = 0.22 \mu\text{m}$, SACS2 dust mix, system radius=5000 AU). Plots on the left are at $i = 90^\circ$ and plots on the right are at $i = 72.5^\circ$. The top two panels show the flux distributions (Stokes I) and the rest show CP, scaled from 10% RCP (dark), to 10% LCP (light). The middle panels show the CP produced by dichroic scattering alone. The bottom panels show the CP after including the effect of dichroic extinction as well. Regions where the flux is low appear noisy in the CP maps.

where CP is highest in the axial field case (due to the large inclination of the grain short axis to the direction of incident photons from the central source).

It is clear the net CP anywhere in the radiation field is zero due to the reflection symmetry of the system about the rotation axis (z-axis). We will call this bilateral symmetry, since this term is often used to describe the symmetry of the human body. Many YSOs have asymmetric nebula, in some cases with one side of the nebula being much brighter than the other (eg. Ageorges et al., 1996; Gledhill et al. 1996; Stapelfeldt et al., 1999). This may be due to inclination of the inner accretion disk (Gledhill 1991), rotating bright spots on the surface of the star (Wood et al., 2000) or non uniform obscuration by dust in the cavity or in the foreground. To maximise the net CP, we consider the extreme case in a simple manner by summing the model circularly polarised flux from two diametrically opposite quadrants of the nebula. (The quadrants are divided by the equatorial plane of the system and the perpendicular plane containing the axis of the system). In Figure 6 we plot the net CP of this idealised asymmetric nebula as a function of wavelength received at points in the near field located 10000 AU from the centre of a system of radius 5000 AU. The wavelengths plotted are those corresponding to the standard astronomical passbands (UBVRIJHK) and 0.22 μm .

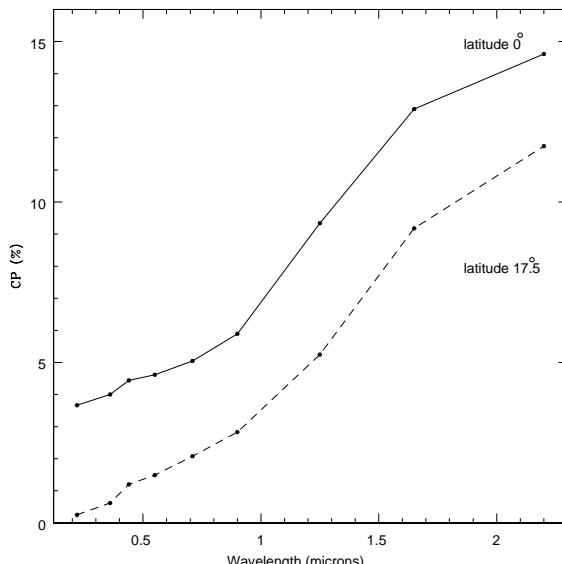


Figure 6. Wavelength dependence of circular polarisation in the vicinity of an YSO with an axial magnetic field. A bilaterally symmetric nebula has zero CP at all wavelengths, so here the CP is summed for two diametrically opposite quadrants of the structure depicted in Figures 4 and 5, providing a simple representation of the CP from a highly asymmetric nebula (see text). The calculation is for points located 10000 AU from the centre of a system with radius 5000 AU, using the SACS2 mix. The optical depth of the YSO envelope is independent of wavelength. Solid line: latitude 0° (i.e. in the equatorial plane). Dashed line: latitude 17.5° . At latitudes $> 17.5^\circ$ the CP is greatly diluted at all wavelengths by direct flux from the star in this model.

It is important to note that we have chosen to model a bipolar structure with constant optical depth (opacity \times density) at all wavelengths, since the strong wavelength dependence of grain opacity would otherwise lead to results which are uninteresting across most of the $0.22 \mu\text{m}$ to $2.2 \mu\text{m}$ wavelength baseline. Very low optical depths lead to an unpolarised radiation field dominated by the central protostar, while very high optical

depths lead to negligible flux escaping the system. Since grain opacity increases from the infrared to the UV, this means the envelope density is lower for the shorter wavelength calculations, in order to preserve the product of opacity and density. We note that only the youngest YSOs, or protostars, display prominent nebulae in the infrared but many of the less dense envelopes of older YSOs (eg. classical T Tauri stars) are expected to appear as circumstellar nebulae in the ultraviolet. Effectively, we are modelling older YSOs in the ultraviolet, and younger YSOs in the infrared.

Exploration of the near field shows that everywhere the net CP $< 5\%$ at $0.22 \mu\text{m}$. This remains true if the flux from just one quadrant or from 3 quadrants is included, or if the more absorptive D2 dust grain mix is used instead of SACS2. Exploration of the envelope parameter space in C, v and cavity opening angle indicates that YSO envelopes with axial fields cannot produce high CP.

3.2.2 Helical Field

In an attempt to increase the CP in the brighter parts of the nebula and avoid the problem of zero net CP in bilaterally symmetric systems, we model a YSO with a helical magnetic field pitched at 45° to the equatorial plane. This is merely a test model, since such a structure is probably unrealistic, but it is easier to understand than the more complicated field structures modelled in the next section. The helical field breaks the bilateral symmetry of the structure because there is a choice between a clockwise or anti-clockwise twist. The system remains axisymmetric (i.e. has rotational symmetry about the z -axis) and is modelled with a 2-D code. An anti-clockwise twist is adopted, as viewed from above the disk plane.

The helical field may be expected to produce high CP in parts of the envelope located at high latitudes via dichroic extinction of the scattered light. Scattering at high latitudes causes linear polarisation mainly in Stokes Q (negative Q by our definition) but in the frame of reference of a grain inclined by 45° to the rotation axis of the system this is Stokes U . Dichroic extinction of the scattered light will therefore produce CP. A narrow cavity opening angle of 25° to the vertical was used, in order to confine the large amount of flux scattered at the cavity walls to high latitudes. For this simulation with the SACS2 mix, dichroic scattering produces relatively low CP in the high latitude regions, since the relevant grain orientations and deflection angles are not optimal.

In Figure 7 we show the results of a simulation of a YSO with a dense envelope ($\tau_{60^\circ} = 22, v = 1.0$) viewed at $i = 72.5^\circ$. These parameters were necessary to create sufficient optical depth in high latitude regions to produce CP by dichroic extinction. The other envelope parameters remain unchanged. The left panel shows the flux distribution seen in the far field, which shows a bipolar nebula in which the dense equatorial regions are entirely hidden from view. A bipolar structure is fairly common among the youngest, most deeply embedded YSOs, such as NGC6334V (Menard et al., 2000). The brightest part of the nebula lies along a diagonal line delineating the cavity wall on the right hand side of the image, due to the larger scattering cross section for photons travelling in that direction from the central star.

In the right hand panel is the CP map, which displays the high CP expected at high latitudes. The CP is highest in the lower (receding) lobe. The net CP produced by this model $0.22 \mu\text{m}$ in the near field reaches 12.8% in the equatorial plane (latitude zero), at 10000 AU from the centre of the system. However, the net CP declines at higher latitudes,

to 6.1% at latitude 17.5° and only 2.2% at latitude 45° . For models with a lower envelope density, as in Figure 5, a helical field leads to $CP < 5\%$ at all points in the near field. Although the high density model has some success in producing high CP, this occurs only in a small portion of the radiation field and the emerging flux level is low. Hence this scenario is not overly encouraging for asymmetric photolysis of prebiotic molecules passing through the radiation field.

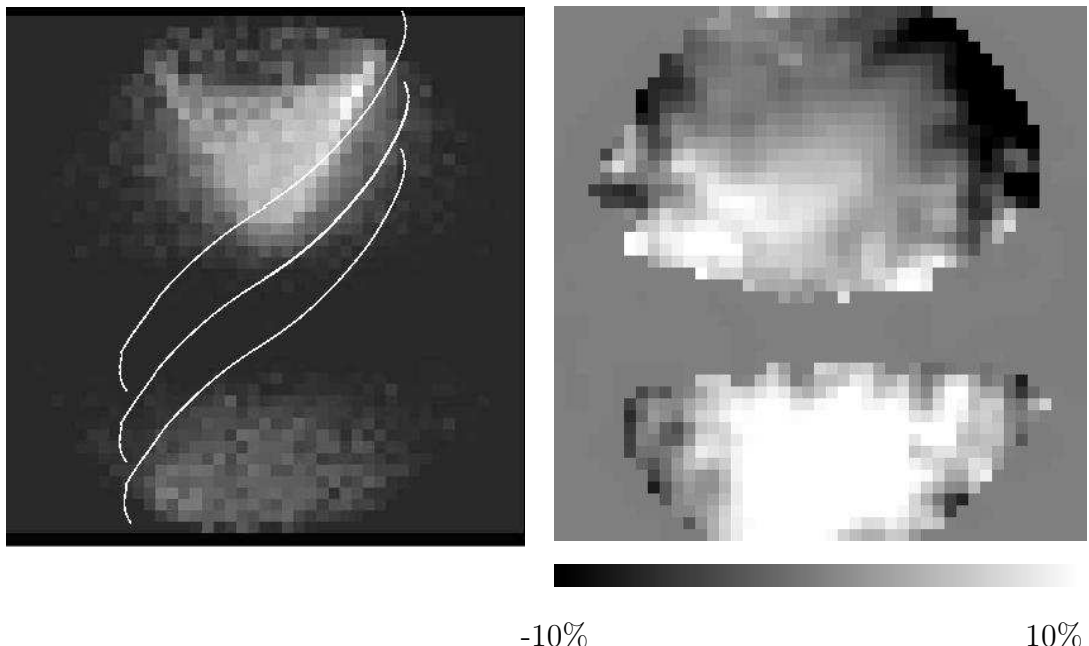


Figure 7. Simulation of a YSO with a dense envelope and a helical field, viewed at $i = 72.5^\circ$. (left) image, with some illustrative field lines superimposed; (right) circular polarisation map. Dichroic extinction produces high CP at high latitudes.

3.2.3 Pinched and Twisted Field

The axial field and helical field models relied upon scattering to produce high CP either (a) directly, via the Z_{41} Stokes matrix element or (b) indirectly, by producing high LP which is subsequently converted to CP by dichroic extinction (K_{34} extinction matrix element). These models produced little net CP largely because the grain mixtures are highly forward throwing at $0.22 \mu\text{m}$: most of the flux is deflected through small angles, leading to little CP or LP by scattering (see section 2.1).

In principle, CP can be produced by dichroic extinction alone, if the magnetic field is twisted (see section 2.2). There are good reasons for presupposing that the magnetic field in the inner part of a YSO system is both pinched and twisted: field lines anchored to the rotating inner accretion disk will naturally become twisted and inside-out gravitational collapse of the parental molecular cloud core will pinch the field, so that it becomes stronger near the central star. In this scenario, the optical density of the envelope can be reduced since direct flux from the central source will become circularly polarised. This scenario is also interesting since the total amount of circularly polarised flux may be higher than in the previous scenarios and the absence of a diluting unpolarised central source removes the restriction to points at low latitude.

The spatial scale and manner in which the putative pinch and twist occurs is unknown, so we have chosen to parameterise the magnetic field in the natural cylindrical polar coordinate system, in order to explore a variety of pinched and twisted structures.

The adopted formalism is:

$$(9) B_r = b_1 z / |z| r^m \exp(-(r^n + a|z|))$$

$$(10) B_z = b_0 + b_1 / a r^{m-1} \exp(-(r^n + a|z|)) (m + 1 - n r^n)$$

$$(11) B_\phi = b_2 z / |z| (1 / (r^q + a z^q + c))$$

where $b_0, b_1, b_2, a, c, n, m$ and q are positive constants which parameterise the field structure. One additional parameter is the unit of length L_B , which was set to values ranging from tens to hundred of AU so that the twist occurs on the scale of the inner parts of the envelope.

At large radii the field becomes axial ($B_z \rightarrow b_0, B_r \rightarrow 0, B_\phi \rightarrow 0$). The signs of B_r and B_ϕ reverse in the plane of the accretion disk ($z=0$) where the pinch and twist is strongest. A discontinuity in the field direction is permitted at $z=0$, implying the existence of a current sheet in the plane of a thin accretion disk. The form of B_z relates to B_r in a manner constrained by the divergence equation (Div $\mathbf{B}=0$). By contrast B_ϕ , the twist component, is independent of the other components since the twist is axisymmetric and therefore does not contribute to the divergence equation.

An example of the field structure produced by Eqs.(9-11) is shown in Figure 8. The parameter space was explored with the Monte Carlo code for cases where the field lines in the circumstellar envelope cross the disk plane only once. Parameters which might potentially produce high net CP were identified by calculating the CP of unscattered (i.e. direct) light from the central star for all system inclinations, i . It was found that structures in which the twist in the field extends throughout the circumstellar envelope produce the highest CP in the direct beam. These correspond to a small value of q (see Eq.11). The optical depth of the envelope and the twist of the field are both greatest at $i = 90^\circ$, so the birefringence of the envelope is greatest in this direction. The maximum of CP in the direct beam usually occurs at a lower angle, where the integrated phase difference between orthogonal electric field components (which gain an initial linear polarisation near the cavity walls) reaches 90° .

In Table 1 we list the net CP produced by an axisymmetric system of 5000 AU radius with the field structure in Figure 8, as a function of inclination. For this model the density structure of Ulrich (1976) is adopted for the YSO envelope (better known as the Terebey, Shu & Cassen (1984) inner solution for the collapse of a rotating isothermal sphere). This structure is similar to Equ.(8) except that the radial density dependence becomes shallower than $R^{-1.5}$ at radii $R \lesssim 3R_c$ (R_c is called the centrifugal radius) approaching $R^{-0.5}$ in the innermost parts of the envelope. This alternative envelope density function was used since the shallower radial density profile spreads the region of highest optical density over a larger volume. Hence, the field is significantly twisted in the dense region where most of the dichroic extinction occurs, which aids the production of CP. In this model $R_c = 100$ AU and $L_B = 40$ AU were adopted. A conical cavity was used, opening at 25° from the vertical, with a radius of 80 AU in the disk plane. The calculation is at $0.22 \mu\text{m}$ for the SACS2 mix.

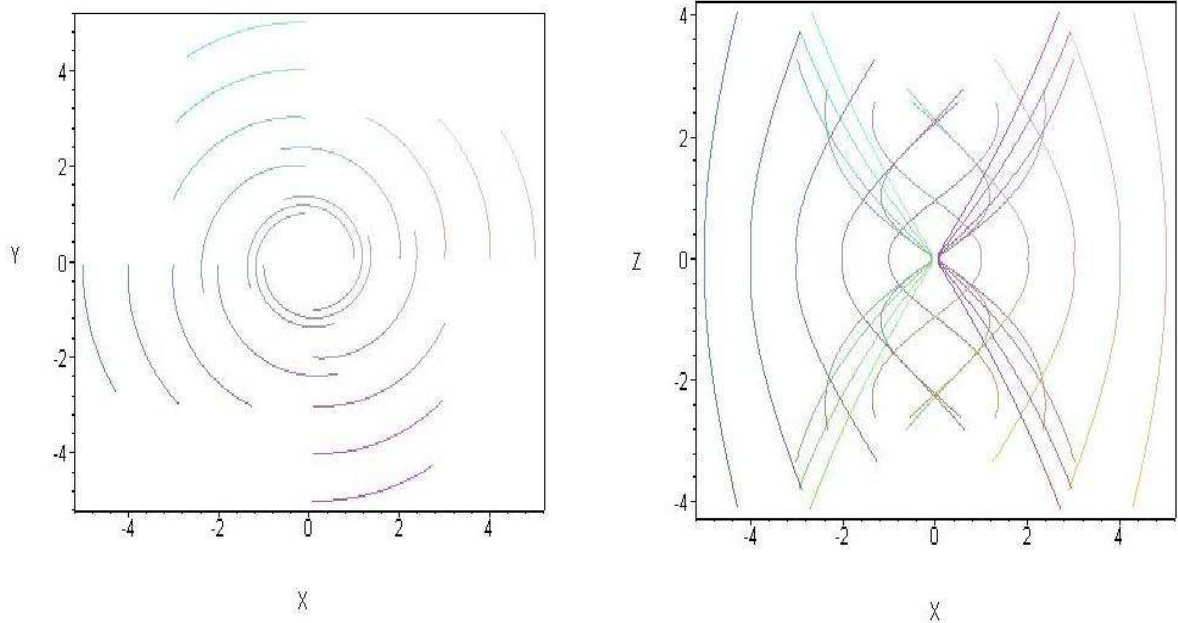


Figure 8. Field structure for $(n=1, m=1, q=1, a=0.4, b_0=0.5, b_1=0.5, b_2=2.0, c=0.1)$, see Eqs.(9-11). The field lines are highly twisted but only weakly pinched. (left) view of the field lines looking down on the disk plane. (right) view from the equatorial plane, showing the pinch more clearly.

Net CP is listed both in the near field at 10000 AU from the central star, and in the far field. Since the optical depth is relatively low ($\tau_{60^\circ} = 3.0$), the CP of the direct beam is also tabulated, since this makes a large contribution to the circularly polarised flux at most inclinations. It is apparent that this field configuration produces high CP in the direct beam at some inclinations but this is diluted by the contribution from scattered light with low CP so that total net CP $< 5\%$ at all points in the external radiation field. If the optical depth is small enough to make dilution by scattered light unimportant ($\tau \lesssim 3$), then the CP of the direct beam is always $< 10\%$ for the SACS2 mix. Optical depth $\tau > 2$ is required to give the beam strong LP ($K_{12}/K_{11} = 0.266$ for the SACS2 mix) and a further optical depth of at least unity is needed to convert a significant fraction of this to CP, even for an ideal field structure, since $K_{34}/K_{11} = 0.156$ for the SACS2 mix.

Extensive exploration of the parameter space (field structure; envelope mass, size, and density structure; cavity size) has not produced a model in which the scattered light has a high net CP. This appears to be due to the large number of paths by which scattered photons can reach a given point in the radiation field, a problem which is in part due to the high albedo (0.6) of the SACS2 mix. As noted earlier, more absorptive grain mixtures such as D1 and D2 have very low values for the K_{34}/K_{11} ratio. Hence, it appears unlikely that YSOs with pinched and twisted magnetic fields can produce high net CP at $0.22 \mu\text{m}$ via dichroic extinction by sub-micron sized grains.

Table 1 - Circular Polarisation from a YSO with a pinched and twisted field

$\cos(i)$	τ^a	CP (direct beam)	Total CP ^b (10000 AU)	Total CP ^b (far field)
0.0	21200	-10.1%	-0.1%	0.0%
0.1	31.9	23.2 %	1.0%	0.9%
0.2	4.6	18.1%	3.2%	3.1%
0.3	3.9	12.5%	4.2%	4.0%
0.4	3.4	8.2%	4.3%	4.0%
0.5	3.0	5.0%	3.7%	3.5%
0.6	2.7	2.7%	2.9%	2.7%
0.7	2.3	1.1%	2.0%	1.9%
0.8	1.7	0.2%	1.2%	1.2%
0.9	0.0	0.0%	0.7%	0.6%
0.9675	0.0	0.0%	1.0%	1.0%
0.9925	0.0	0.0%	1.0%	1.0%

Notes: (a) τ is the optical depth to the central star for the given inclination.

(b) Total CP includes the contributions from direct and scattered light.

3.3 Scenario 2a - two uniform sheets of nebulosity with inclined fields

In Section 2.2 we showed how a uniform slab of cloud can produce CP via dichroic extinction of a linearly polarised beam. The linear polarisation of the incident beam could arise from scattering or prior dichroic extinction. Here we show the results of a Monte Carlo simulation of the latter scenario: light passing through 2 parallel uniform sheets containing dust grains which are perfectly aligned with uniform magnetic fields (see Figure 9). The fields in each slab are parallel to the plane of the slab but inclined to each other by some angle ζ . The CP of the emerging radiation, including the contribution from scattered light, is listed in Table 2 as a function of cloud optical depth (τ), distance beyond the second cloud (d) and ζ , using the SACS1 grain mixture. This scenario is similar to earlier calculations by Martin (1974) but modern computing power allows us to include the important effects of scattered light.

It is clear that this scenario produces fairly high CP ($\approx 10\%$) with the SACS1 mix. The total CP is lower than for the idealised case shown in Figure 3, since the the first slab produces $< 100\%$ LP and scattered light dilutes the CP produced by the direct beam. Scattering tends to remove the memory of the incident polarisation state, so multiply scattered photons (sometimes scattered several times within a slab) usually have lower CP than singly scattered photons or the direct beam in these simulations. For the SACS1 mix the typical albedo is 0.61 (albedo varies slightly with grain orientation), so the average number of scatterings in an optically thick nebula is $1/(1 - 0.61) \approx 2.5$. As noted in Section 3.2.3, the D1 mix produces much lower CP despite its low albedo, since the birefringence of more absorptive grains is much lower ($K_{34}/K_{11} = 0.043$, see also Figure 2). The requirements for this scenario to produce high CP are therefore:

- A well ordered field structure in both of the cloud sheets, the two clouds having field directions which are significantly different. In the case of random field orientations,

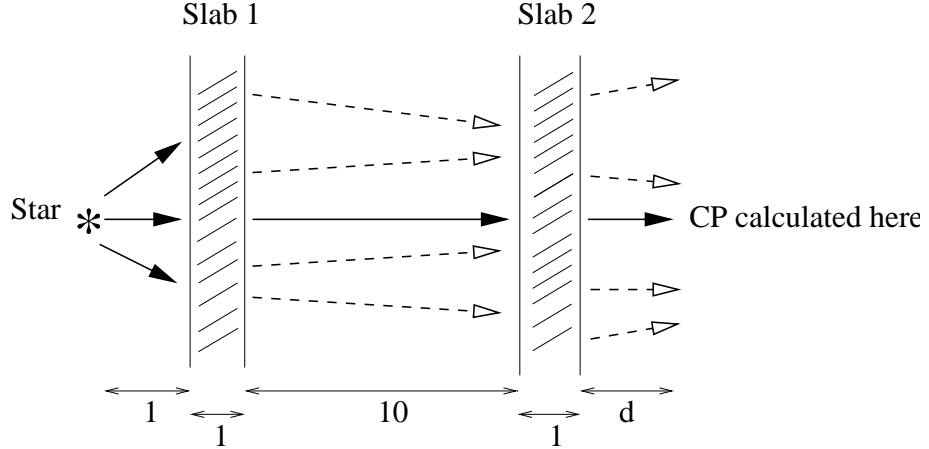


Figure 9. Cartoon illustrating Scenario 2a. The direct beam from the star perpendicular to the slabs is shown as a solid line; the dashed lines illustrate rays of scattered light. Both slabs of nebulosity contain perfectly aligned oblate spheroids with magnetic fields orthogonal to the direct beam. The field directions are inclined to each other by an angle ζ in the plane of the slabs. CP is calculated along the line of the direct beam at various distances, d , beyond slab 2. Distance units are arbitrary.

half of all pairs of cloud sheets would have field inclinations within 22.5° of $\zeta = 45^\circ$ or $\zeta = 135^\circ$, leading to high Cpol.

- A grain mixture with a small imaginary component of refractive index (i.e. a shiny mixture), which is quite likely for a mixture dominated by eg. silicates and water ice in star forming regions.

Table 2 - Circular Polarisation from Scenario 2a

τ^a	ζ	CP (direct beam)	Total CP ($d=1$)	Total CP ($d=10$)	Total CP ($d=20$)
1	0°	0%	0.0%	0.0%	0.0%
2	0°	0%	0.0%	0.0%	0.0%
3	0°	0%	0.0%	0.0%	0.0%
4	0°	0%	0.0%	0.0%	0.0%
1	15°	2.52%	0.68%	1.33%	1.73%
2	15°	6.77%	2.10%	3.70%	4.32%
3	15°	9.24%	2.59%	5.01%	5.55%
4	15°	9.64%	3.52%	3.93%	4.68%
1	30°	4.50%	1.06%	2.51%	3.06%
2	30°	12.9%	3.86%	6.56%	8.23%
3	30°	18.5%	5.13%	7.67%	9.52%
4	30°	19.9%	3.69%	7.36%	8.39%
1	45°	5.43%	1.64%	3.23%	3.59%
2	45°	17.1%	5.72%	8.65%	9.41%
3	45°	27.0%	6.75%	10.5%	11.8%
4	45°	31.2%	5.39%	9.27%	9.33%

(a) τ is the optical depth through each slab for unpolarised light.

3.4 Scenario 2b - a YSO and a cloud sheet

The alternative scenario whereby the LP is produced by scattering is also possible. The D2 mix produces a maximum LP up to 90% at $0.22\text{ }\mu\text{m}$ by single scattering for deflection angles near 90° (with the oblate grains oriented face on to the incident ray). Similarly, the SACS1, SACS2, and D1 mixes can produce LP up to 76%, 74% and 88% respectively. However, the difficulty for scattering models remains the tendency for forward scattering in the ultraviolet, which causes most of the scattered flux to have much lower LP. To produce a radiation field with high LP it is therefore necessary to construct a scenario in which light from an unpolarised source (eg. a star) is scattered through $\sim 90^\circ$ but direct flux from the source is somehow obscured, in order to prevent dilution.

Scattering in the lobes of a bipolar nebula is one example of such a scenario. YSO envelopes viewed at $i \approx 90^\circ$ appear as bipolar nebulae with the central star obscured, as shown in Figure 7 for the case of a helical field. The scattered light from a bipolar nebula has significant LP which is mostly parallel to the disk plane, provided dichroic effects are unimportant. (Competition between dichroic extinction and dichroic scattering tends to reduce the degree of polarisation).

To quantify the LP at $0.22\text{ }\mu\text{m}$, Monte Carlo simulations of an axisymmetric system were run for YSOs with spherical grains (so that there are no dichroic effects), for both low density and high density envelopes described by Equ.(8). Results are given in Table 3. Grains with the size distribution and optical properties of the D2 mix were used to help produce high LP. The relatively low albedo of the D2 mix, 0.43, means that the emergent radiation is dominated by singly scattered light, which tends to have higher LP than multiply scattered light. A narrow cavity opening angle of 20° to the vertical was used in order to ensure that most of the emerging flux is polarised parallel to the disk plane (negative Q), sampling only a small sector of the centrosymmetric pattern. The resulting flux distributions for the low density and high density simulations were similar to those shown in the top panels of Figure 5 and the left panel of Figure 7 respectively.

The results in Table 3 show that LP of up to 30% is produced in systems with high optical depth, viewed at $i = 90^\circ$. In systems with relatively low optical depth more flux is able to emerge after scattering at low latitudes, so the forward throwing phase function significantly reduces the LP. If the YSO has an active molecular outflow, there may be a modest optical depth of dust in the cavity, which would increase the scattering at high latitudes with polarisation parallel to the disk plane. After adding a uniform dust component in the cavity, with optical depth of 0.75 along the axis from the protostar to the edge of the system, the maximum LP was raised from 30.8% to 39.4% in the $\tau_{60^\circ} = 36; v = 1.0$ case.

It is clear that a bipolar nebula producing almost 40% LP at $\lambda = 0.22\text{ }\mu\text{m}$ could lead to fairly high CP after dichroic extinction by an interstellar cloud sheet, as in Scenario 2a. However, there are some reasons why Scenario 2(a) might be preferred over 2(b): first, in 2(b) the highest LP is produced in the weakest part of the radiation field around a very optically thick nebula; second, the LP produced by scattering in an optically thick nebula is lower than that produced by dichroic extinction (see Figure 3).

Table 3 - far field LP from a bipolar YSO with spherical grains

Model	cos(i)	LP
$\tau_{60^\circ} = 36; v = 1.0$	0.0	30.8%
$\tau_{60^\circ} = 36; v = 1.0$	0.5	18.2%
$\tau_{60^\circ} = 5.9; v = 1.0$	0.0	17.8%
$\tau_{60^\circ} = 5.9; v = 1.0$	0.5	5.1% ^a

Note: (a) LP is strongly diluted by flux from the central source at $i \lesssim 60^\circ$.

4 CP in Orion and implications for grain axis ratio

In this section we model the high CP measured at infrared wavelengths in Orion, to see what insights can be gained for application to UV modelling. The BNKL-SEBN region of Orion displays the centrosymmetric pattern of LP vectors normally associated with scattering, rather than the aligned vectors associated with dichroic extinction. The situation in NGC6334V (the other known case of high infrared CP) is unclear, since the nebulous region is too small for a clear LP pattern to be determined. There is no doubt that BNKL-SEBN is a reflection nebula but it is quite possible that the CP of the radiation from this nebula is due to dichroic extinction of the scattered light: at infrared wavelengths linear dichroism has less effect on the polarisation state than birefringence (see Figure 2 and Martin 1974). Hence, high CP can be produced without much disturbance of the centrosymmetric vector pattern.

We illustrate this with an infrared model of the BNKL-SEBN region in Figure 10, which shows the CP and LP produced by a variation on the SACS1 grain mix, using grains with axis ratio of only 1.5:1. For this model a forced scattering code 'shadow.f' was used, which is described in Lucas et al.(2003). The magnetic field direction in the plane of the sky has been measured by Chrysostomou et al.(1994) via high spatial resolution observation of the 2.12 μm H₂ emission in the region. The data indicates that the grain alignment axis is tilted by approximately 60° to the Poynting vector of rays from the illuminating source IRc2. This orientation is suitable for production of CP by either dichroic extinction or dichroic scattering. In this simple model we assume that the magnetic field lies exactly in the plane of the sky and that IRc2 and BNKL-SEBN lie at the same distance from the Earth, so that the scattering angle is 90°. The light from SEBN is then passed through a uniform slab of cloud in the foreground with the same field orientation, which amplifies the dichroic extinction occurring within SEBN itself. The existence of this foreground extinction is inferred from the 1.25 μm data of Chrysostomou et al.(2000), in which the entire region is obscured from view (see also Brand et al., 1988). The left panel of Figure 10 shows that the observed CP of 15-20% at 2.2 μm (see Chrysostomou et al., 2000) is reproduced by this model, while the centrosymmetric LP pattern observed by Minchin et al.(1991) is also reproduced (right hand panel). The centrosymmetric pattern also acts as a constraint on dichroic scattering models, since scattering by highly flattened grains also produces some alignment of the vectors, perpendicular to the alignment caused by dichroic extinction (eg. Whitney & Wolff 2002; Lucas 2003).

In fact this is an imperfect model since the predicted degree of LP at 2.2 μm (90%) is far higher than the observed value (38% at 2.2 μm and 57% at 3.6 μm), owing to the 90°

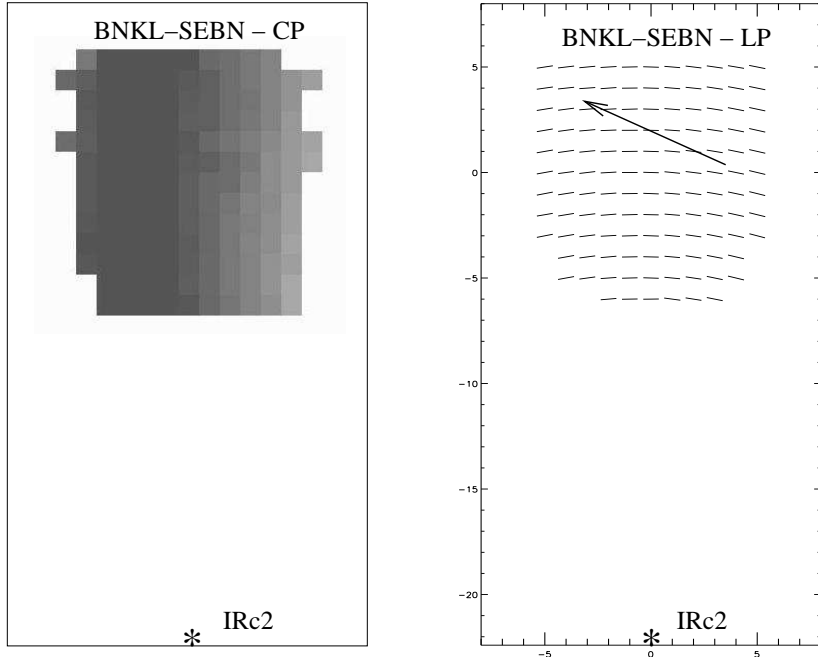


Figure 10. A simple infrared model of BNKL-SEBN. In this simple model the nebulous cloud BNKL-SEBN is illuminated by the YSO IRc2. Scattering by oblate spheroids with axis ratio 1.5:1 reproduces the centrosymmetric pattern (right panel) observed by Minchin et al., (1991). Dichroic extinction by a foreground sheet of cloud and BNKL-SEBN itself reproduces the maximum observed CP of 15-20% (left panel) without perturbing the LP vectors by more than 2° . The magnetic field direction in SEBN and the foreground sheet (tilted at 60° to the incident rays from IRc2) is indicated by the arrow in the right hand panel.

scattering angle. To improve the model we varied 5 parameters: scattering angle, maximum grain size, grain axis ratio, optical depth and the magnetic field orientation. Three classes of successful solution were found, all of which reproduce to a close approximation the 4 observables described above (CP percentage; LP centrosymmetry; percentage and wavelength dependence of LP). The three classes of solution are:

- CP produced mainly by dichroic extinction.
- CP produced mainly by dichroic scattering.
- CP having significant contributions from both mechanisms.

With such a diversity of solutions it is not possible to determine which mechanism has produced the observed CP. We note however, that grain axis ratios of only 1.5:1 (and perhaps less) are sufficient to produce successful solutions by dichroic extinction, whereas axis ratios approaching 3:1 are needed for solutions in which dichroic scattering dominates (see section 3.1). Previous estimates have allowed axis ratios in the range from 1.1 to 3 in the BN-KL region (eg. Hildebrand & Dragovan 1995), so a 3:1 ratio cannot be ruled out. Nevertheless, the smaller grain ratios associated with dichroic extinction solutions are more consistent with the typical values derived from linear polarimetry of star formation regions.

With regard to production of UV CP, a grain axis ratio less than the value of 3 used earlier in this work would not necessarily reduce the degree of polarisation. The successful scenario 2(a), and others dependent on dichroic extinction, can compensate for a smaller axis ratio by using an increased optical depth. Inspection of the extinction matrix elements indicates that if the SACS1 mix were used with an axis ratio of 2, the

optical depth would have to be increased by a factor of only 1.56, (eg. from $\tau = 3$ per slab of cloud to $\tau = 4.7$) in order to produce the same CP. However, for an axis ratio of 1.5, the optical depth would have to be increased by a factor of 2.70 (corresponding to $\tau = 8.1$ per slab), which would reduce the emergent flux even from very luminous O-type stars to the point where other light sources would probably dominate the local radiation field, at least in crowded star forming regions like Orion. Thus, an axis ratio of 2 is no obstacle to production of $\sim 10\%$ net UV CP, but with an axis ratio of 1.5 or less the UV CP is unlikely to exceed 5 or 6%.

5 Discussion

We have explored a number of scenarios which attempt to produce high CP in star formation regions via dichroic scattering and/or dichroic extinction. Scenarios which rely principally upon dichroic extinction have produced UV net CP $\approx 10\%$. This is lower than the CP produced in infrared models owing to the much lower birefringence in the UV for plausible grain size distributions (see Figure 2). The unscattered component of the radiation field can have net CP $\geq 20\%$ in the UV (see Table 1 and Table 2) but the scattered component reduces the overall CP in the scenarios considered here. Scenarios which rely principally on dichroic scattering rather than dichroic extinction are much less successful, due to the forward throwing ultraviolet phase function. A scenario not considered here is that a low mass YSO or T Tauri star might produce high ultraviolet CP in parts of its own envelope. Computation of this mode by Wolff et al.(2000) with spherical grains yielded very low CP due to the symmetry of the system but computation with aligned non spherical grains has yet to be explored. It should be noted that this work does not exhaust all the possibilities for production of high UV CP, so we do not attempt to put an upper limit on the CP which may occur in star formation regions.

The production of 10% UV CP is still sufficient to be encouraging for the hypothesis that CP in star forming regions may produce an initial enantiomeric excess in prebiotic molecules by asymmetric photolysis. A CP of 10% can be produced by dichroic extinction even if the grain axis ratio is only 2:1 (see Section 4). Furthermore, in Scenarios 2(a) and 2(b) (which involve dichroic extinction by one or more interstellar cloud sheets) the CP of the radiation field in locations well beyond the final cloud sheet does not vary strongly with spatial position. This is an attractive feature for crowded star forming regions such as Orion, where YSOs are in constant motion. (Close encounters between YSOs on 10^4 AU scales are fairly common in Orion (Scally & Clarke 2001) and last $\sim 10^4$ yr for typical relative velocities of 3 kms^{-1}). By contrast, in the scenarios considered in section 3.2, in which the CP is produced in the envelope of a high mass YSO, a passing proto-sun would often experience CP which varies significantly in space, and in many cases the incident LCP and RCP integrated over the path would average to near zero.

The efficiency of asymmetric photolysis as a function of CP percentage is not well quantified at present. Experiments by Bonner & Dean (2000) show that elliptically polarised light produces a smaller enantiomeric excess than 100% circularly polarised light. Their optical system with the principal axis of a quarter waveplate inclined at $22^\circ.5$ to the polarisation plane of a 100% linearly polarised beam should theoretically have produced 70.7% CP and 70.7% LP (the Stokes vector elements add in quadrature to 100%). The measured enantiomeric excess produced in Leucine with this set-up was 73-83% of

that produced by 100% circularly polarised light, which tends to support a roughly linear relationship with CP, defined as $CP=|V/I|$. Further experiments of this type would be very useful.

We note that circular dichroism has not yet been measured for the amino acids found in meteorites (see Bailey 2001) but experiments with other amino acids (Flores et al., 1977), albeit dissolved in solution, suggest that CP well in excess of 10% is necessary to produce the large enantiomeric excesses measured in meteorites. Even 99% asymmetric photolysis by radiation with 10% CP would produce an excess which is below 1%, unless the enantiomeric excess vs. CP relationship is highly non linear. It is possible that asymmetric photolysis in star forming regions acts first on molecules with higher circular dichroism, and the resulting enantimERIC excess is then transferred chemically to other chiral molecules. For example, some of the 'amino acids' in the Murchison meteorite are present only as precursor molecules with unknown circular dichroism. They become amino acids only upon extraction by acid hydrolysis. However, the enantiomeric excess of up to 15% in isovaline measured in the Murchison meteorite remains problematic. Terrestrial homochirality is easier to explain at least, since experiments by Shibata et al.(1998) have shown that a small initial enantiomeric excess can be greatly amplified by asymmetric autocatalysis.

CP attributed to the dichroic extinction mechanism has been observed towards many astrophysical sources, as discussed in Section 1. However, it is important to increase the size of the observational database, in order to search for clear examples of CP production by dichroic extinction in star formation regions. Observation at shorter wavelengths ($\leq 1.25 \mu\text{m}$) would be helpful since significant alignment of the LP vectors would then be expected in regions of high CP, owing to the increase in the K34/K12 ratio (see Figure 2). Any alignment caused by dichroic scattering would be in the perpendicular direction. The CP produced by twisting magnetic fields in the diffuse interstellar medium along lines of sight toward main sequence stars is $\ll 1\%$, eg. Kemp & Wolstencroft (1972). However, the much higher densities found in star formation regions are likely to produce higher CP. We note that a large scale survey of star formation regions in the southern sky is currently planned with the Japanese Infrared Survey Facility in South Africa.

Acknowledgements

"This work was carried out on the Miracle Supercomputer, at the HiPerSPACE Computing Centre, UCL, which is funded by the U.K. Particle Physics and Astronomy Research Council. We thank Janneke Balk of the Oxford University Biochemistry Department, Mike Wolff of the Space Telescope Science Institute, Jeremy Yates of University College London and Dave Aitken at the University of Hertfordshire for helpful advice and discussions. We particularly thank Jim Collett of UHerts for helping us to develop parameterised magnetic field structures. We are also grateful to the referee for a helpful report. PWL is supported by a PPARC Advanced Fellowship."

References

- Ageorges, N., Fischer, O., Stecklum, B., Eckart, A., Henning, T.: 1996, The Chamaeleon Infrared Nebula: A Polarization Study with High Angular Resolution, *Astrophys. J. Letters* 463, pp. 101-104

Bailey, J., Chrysostomou, A., Hough, J.H., Gledhill, T.M., McCall, A., Clark, S., Menard, F., and Tamura, M.: 1998, Circular Polarization in Star-Formation Regions: Implications for Biomolecular Homochirality, *Science* 281, 672-674

Bailey, J.: 2001, Astronomical Sources of Circularly Polarised Light and the Origin of Homochirality, *Orig. Life and Evol. Biosphere* 31, 167-183

Barber, P.W. and Hill, S.C.: 1990, *Light Scattering by Particles: Computational Methods*, World Scientific, New York

Bonner, W.A.: 1991, The Origin and Amplification of Biomolecular Chirality, *Orig. Life and Evol. Biosphere* 21, 59-111

Bonner, B.A. and Dean, B.D.: 2000, Asymmetric Photolysis with Elliptically Polarised Light, *Orig. Life and Evol. Biosphere* 30, 513-517

Brack, A.: 1998, *The Molecular Origins of Life*, CUP, Cambridge, pp. 1-11

Brand, P.W.J.L., Moorhouse, A., Burton, M.G., Geballe, T.R., Bird, M., and Wade, R.: 1988, Ratios of molecular hydrogen line intensities in shocked gas: evidence for cooling zones, *Astrophys. J. Letters* 334, 103-106

Cardelli, J.A., Clayton, G.C., and Mathis, J.S.: 1989, The relationship between infrared, optical, and ultraviolet extinction, *Astrophys. J.* 345, 245-256

Chiang, E.I., Joung, M.K., Creech-Eakman, M.J., Qi, C., Kessler, J.E., Blake, G.A., and van Dishoeck, E.F.: 2001, Spectral Energy Distributions of Passive T Tauri and Herbig Ae Disks: Grain Mineralogy, Parameter Dependences, and Comparison with Infrared Space Observatory LWS Observations, *Astrophys. J.* 547, 1077-1089

Chrysostomou, A., Hough, J.H., Burton, M.G., and Tamura, M.: 1994, Twisting magnetic fields in the core region of OMC-1, *Mon. Not. R. Astron. Soc.* 268, 325-334

Chrysostomou, A., Menard, F., Gledhill, T.M., Clark, S., Hough, J.H., McCall, A., Tamura, M.: 1997, Polarimetry of young stellar objects - II. Circular polarization of GSS 30, *Mon. Not. R. Astron. Soc.* 285, 750-758

Chrysostomou, A., Gledhill, T.M., Menard, F., Hough, J.H., Tamura, M., and Bailey, J.: 2000, Polarimetry of Young Stellar Objects - III. Circular Polarimetry of OMC-1, *Mon. Not. R. Astron. Soc.* 312, 103-115

Cronin, J.R. and Pizzarello, S.: 1997, Enantiomeric excesses in meteoritic amino acids, *Science* 275, 951-955

Draine, B.T.: 1985. Tabulated optical properties of graphite and silicate grains, *Astrophys. J. Supplement* 57, 587-594

Engel, M.H. and Macko, S.A.: 1997, Isotopic evidence for extraterrestrial non-racemic amino acids in the Murchison meteorite, *Nature* 389, 265-268

Fischer, O., Henning, Th., and Yorke, H.W.: 1994, Simulation of polarization maps. 1: Protostellar envelopes, *Astron. Astrophys.* 284, 187-209

Flores, J.J., Bonner, W.A. and Massey, G.A.: 1977, Asymmetric Photolysis of (RS)-Leucine with Circularly Polarised Ultraviolet Light, *J. Am. Chem. Soc* 99, 3622-3625

Gledhill, T.M.: 1991, Linear polarization maps of bipolar and cometary nebulae - A polarized source interpretation, *Mon. Not. R. Astron. Soc.* 252, 138-150

Gledhill, T.M., Chrysostomou, A., and Hough, J.H.: 1996, Linear and circular imaging polarimetry of the Chamaeleon infrared nebula, *Mon. Not. R. Astron. Soc.* 282, 1418-1436

Gledhill, T.M. and McCall, A.: 2000. Circular polarization by scattering from spheroidal dust grains, *Mon. Not. R. Astron. Soc.* 314, 123-137

Hamann, F. and Persson, S.E.: 1992, Emission-line studies of young stars. III - Correlations with the infrared excess, *Astrophys. J.* 394, 628-642

Hildebrand, R.H., and Dragovan, M.: 1995, The shapes and alignment properties of interstellar dust grains, *Astrophys. J.* 450, 663-666

Hillenbrand, L.A., Strom, S.E., Vrba, F.J., Keene, J.: 1992, Herbig Ae/Be stars - Intermediate-mass stars surrounded by massive circumstellar accretion disks, *Astrophys. J.* 397, 613-643

Hough, J.H. and Aitken, D.K.: 2003, Polarimetry in the infrared: what can be learned? *J. Quantitative Spectroscopy and Radiative Transfer* 79-80, 733-740

Joyce, G.F., Vosser, G.M., van Boeckel, C.A.A., van Boom, J.H., Orgel, L.E., van Westrenen, J.: 1984, Chiral Selection in poly(C)-directed synthesis of oligo(G), *Nature* 310, 602-604.

Kemp, J.C. and Wolstencroft, R.D.: 1972, Interstellar Circular Polarization: Data for Six Stars and the Wavelength Dependence, *Astrophys. J. Letters* 176, 115-118

Lazarian, A. Mechanical Alignment of Suprothermal Grains: 1995, In: Roberge, W.G., Whittet, D.C.B., editors. *Polarimetry of the Interstellar Medium.* ASP conf. series 97, pp. 425-429.

Lazarian, A. Physics of Grain Alignment. In: Franco, J., Terlevich, L., Lpez-Cruz, O., Artxaga, I.: 2000, editors. *Cosmic Evolution and Galaxy Formation: Structure, Interactions, and Feedback.* ASP conf. series 215, pp. 69-78

Lonsdale, C.J., Dyck, H.M., Capps, R.W., Wolstencroft, R.D.: 1980, Near-infrared circular polarization observations of molecular cloud sources, *Astrophys. J. Letters* 238, 31-34

Lucas, P.W. and Roche, P.F.: 1998, Imaging Polarimetry of Class I young stellar objects, *Mon. Not. R. Astron. Soc.* 299, 699-722

Lucas, P.W.: 2003, Computation of Light Scattering in Young Stellar Objects, *J. Quantitative Spectroscopy and Radiative Transfer* 79-80, 921-938

Lucas, P.W., Fukagawa, M., Tamura, M., Beckford, A., Itoh, Y., Murakawa, K., Suto, H., and Hayashi, S.S.: 2003, Near IR polarimetry and Magnetic Field Structure in HL Tau (in prep)

Kim, S.-H., Martin, P.G. and Hendry, P.D.: 1994. The size distribution of interstellar dust particles as determined from extinction, *Astrophys. J.* 422, 164-175

Martin, P.G., Illing, R., and Angel, J.R.P.: 1972. Discovery of interstellar circular polarization in the direction of the Crab nebula, *Mon. Not. R. Astron. Soc.* 159, 191-201

Martin, P.G.: 1974, Interstellar polarization from a medium with changing grain alignment, *Astrophys. J.* 187, 461-472

Mathis, J.S., Rumpl, W., Nordsieck, K.H.: 1977, The size distribution of interstellar grains, *Astrophys. J.* 217, 425-433

Menard, F., Chrysostomou, A., Gledhill, T.M., Hough, J.H., Bailey, J.: 2000, In: Lemarchand, G. and Meech, K.(eds.) 'Bioastronomy 99: A New Era in the Search for Life in the Universe' (San Francisco) ASP conf. series 213, pp. 355-358

Minchin, N.R., Hough, J.H., McCall, A., Burton, M.G., McCaughrean, M.J., Aspin, C., Bailey, J.A., Axon, D.J., and Sato, S.: 1991a, Near infrared imaging polarimetry of bipolar nebulae - I. The BN-KL region of OMC-1, *Mon. Not. R. Astron. Soc.* 248, 715-729

Minchin, N.R., Hough, J.H., Burton, M.G., and Yamashita, T.: 1991b, Near-infrared imaging polarimetry of bipolar nebulae. IV - GL 490, GL 2789 and GL 2136, *Mon. Not. R. Astron. Soc.* 251, 522-528

Mishchenko, M.I., Hovenier, J.W., Travis, L.D.: 2000, *Light Scattering by Nonspherical Particles: Theory, Measurements, and Applications* Academic Press, San Diego, 2000.

O'Dell, C.R., and Wen, Z.: 1994, Postrefurbishment mission Hubble Space Telescope images of the core of the Orion Nebula: Proplyds, Herbig-Haro objects, and measurements of a circumstellar disk, *Astrophys. J.* 436, 194-232

Pizzarello, S. and Cronin, J.R.: 2000, *Geochim. Cosmochim. Acta* 64, 329-338

Pollack, J.B., Hollenbach, D., Beckwith, S., Simonelli, D.P., Roush, T., Fong, W.: 1994, Composition and radiative properties of grains in molecular clouds and accretion disks. *Astrophys. J.* 421, 615-639

Preibisch, Th., Ossenkopf, V., Yorke, H.W., and Henning, Th.: 1993, The Influence of ice-coated grains on protostellar spectra, *Astron. Astrophys.* 279, 577-588

Purcell, E.M.: 1979, Suprothermal rotation of interstellar grains, *Astrophys. J.* 231, 404-416

Roberge, W.G.: 1995, Grain Alignment in Molecular Clouds. In: Roberge, W.G., Whittet, D.C.B., editors. *Polarimetry of the Interstellar Medium*. ASP conf. series 97, pp. 401-418.

Roberts, J.A.: 1984, Supernovae and Life, *Nature* 308, 318

Rubenstein, E., Bonner, W.A., Noyes, H.P., Brown, G.S.: 1983, Supernovae and Life, *Nature* 306, 118

Scally, A. and Clarke, C.: 2001, Destruction of protoplanetary discs in the Orion Nebula Cluster, *Mon. Not. R. Astron. Soc.* 325, 449-456

Shafter, A. and Jura, M.: 1980, Circular polarization from scattering by circumstellar grains, *Astronom. J.* 85, 1513-1519

Shakura, N.I., and Sunyaev, R.A.: 1973, Black holes in binary systems. Observational appearance, *Astron. Astrophys.* 24, 337-355

Shibata, T., Yamamoto, J., Matsumoto, N., Yonekubo, S., Osanai, S., and Soai, K.: 1998, Amplification of a Slight Enantiomeric Imbalance in Molecules based on Asymmetric Autocatalysis: the first correlation between high enantiomeric enrichment in a chiral molecules and circularly polarised light, *J. Am. Chem. Soc.* 120, 12157-12158

Smith, C.H., Wright, C.M., Aitken, D.K., Roche, P.F., and Hough, J.H.: 2000, Studies in mid-infrared spectropolarimetry - II. An atlas of spectra, *Mon. Not. R. Astron. Soc.* 312, 327-361

Sorrell, W.H.: 1990, The 2175-A feature from irradiated graphitic particles, *Mon. Not. R. Astron. Soc.* 243, 570-587

Stapelfeldt, K.R.; Watson, A.M., Krist, J.E., Burrows, C.J., Crisp, D., Ballester, G.E., Clarke, J.T., Evans, R.W., Gallagher, J.S.III, Griffiths, R.E., Hester, J.J., Hoessel, J.G., Holtzman, J.A., Mould, J.R., Scowen, P.A., Trauger, J.T.: 1999, A Variable Asymmetry in the Circumstellar Disk of HH 30, *Astrophys. J. Letters* 516, 95-98

Tamura, M., Hough, J.H., Hayashi, S.S.: 1995, 1 Millimeter Polarimetry of Young Stellar Objects: Low-Mass Protostars and T Tauri Stars, *Astrophys. J.* 448, 346-355

Ulrich, R.K.: 1976, An infall model for the T Tauri phenomenon, *Astrophys. J.* 210, 377-391

Whitney, B.A., and Wolff, M.: 2002, Scattering and Absorption by Aligned Grains in Circumstellar Environments, *Astrophys. J.* 574, 205-231

Whittet, D.C.B.: 1992, *Dust in the Galactic Environment*, pub IOP, London, pp. 79-104

Wright, C.M.: 1994, *Mid-Infrared Spectropolarimetry of Molecular Cloud Sources: Magnetic Fields and Dust Properties* PhD thesis, Univ. College, Univ. of New South Wales, Sydney

Wolff, M.J., Whitney, B.A., Clayton, G.C., Ferris, J.P., Whittet, D.C.B. and Sofia, U.J.: 2000, Circular Polarization in Protostellar and pre-Main Sequence Environments: Implications for Enantiomeric Excesses in Amino Acids, in proc. *First Astrobiology Science Conference* NASA/Ames Research Center, pp. 116-119

Wood, K. and Reynolds, R.J.: 1999, A Model for the Scattered Light Contribution and Polarization of the Diffuse H α Galactic Background, *Astrophys. J.* 525, 799-807

Wood, K., Wolk, S.J., Stane, K.Z., Leussis, G., Stassun, K., Wolff, M., and Whitney, B.: 2000, Optical Variability of the T Tauri star HH30 IRS, *Astrophys. J. Lett.* 542, L21-24